Vector parameters in atomic ionization by twisted light: Polarization of the electron and residual ion

Maksim D. Kiselev *
Skobeltsyn Institute of Nuclear Physics, Lomonosov Moscow State University, 119991 Moscow, Russia;
Faculty of Physics, Lomonosov Moscow State University, 119991 Moscow, Russia;
School of Physics and Engineering, ITMO University, 197101 Saint Petersburg, Russia;
and Laboratory for Modeling of Quantum Processes, Pacific National University, 680035 Khabarovsk, Russia

Elena V. Gryzlova
Skobeltsyn Institute of Nuclear Physics, Lomonosov Moscow State University, 119991 Moscow, Russia

Alexei N. Grum-Grzhimailo
Skobeltsyn Institute of Nuclear Physics, Lomonosov Moscow State University, 119991 Moscow, Russia
and School of Physics and Engineering, ITMO University, 197101 Saint Petersburg, Russia

(Received 6 October 2023; accepted 18 January 2024; published 7 February 2024)

The electron and ion properties observed in photoionization inherit the symmetry properties of both a target and radiation. Introducing symmetry breaking in the photoionization process, one can expect to observe a noticeable variation of the vector correlation parameters of either an outgoing photoelectron or a residual ion. One of the ways to violate symmetry is to irradiate matter by twisted radiation, which involves an additional screw. In the paper we present an extension of the approach developed in Phys. Rev. A **108**, 023117 (2023) for photoelectron angular distribution to the other vector correlation parameters, specifically, photoelectron spin polarization, orientation, and alignment of the residual ion. Usually two conditions are needed to produce polarized photoelectrons: a system possesses a helix and a presence of noticeable spin-orbital interaction. Here, we investigate whether a twisted light brings an additional helicity to a system. As an illustrative example we consider ionization of a valence $4p$ shell of atomic krypton by circularly and linearly polarized Bessel light. The photoelectron spin components are analyzed as a function of the cone angle of twisted radiation.

DOI: 10.1103/PhysRevA.109.023108

I. INTRODUCTION

The technique of laser radiation generation has been developing in very diverse directions to reach higher frequencies, brighter intensities, shorter durations, pulse with a chirp, or a definite carrier envelope phase (CEP). Among these, twisted light—i.e., pulses with definite projection of orbital angular momentum possessing a nonuniform intensity profile structure, a complex surface of the constant phase, and internal flow patterns—plays an important role [1,2]. Today a twisted light is available in a broad range of energies from the optical region up to the vacuum ultraviolet (VUV) range [3–12]. A manifold of generation techniques have been developed and successfully applied: spiral phase plates [13,14], holograms [15], q plates [16], axicons [17], integrated ring resonators [18], on-chip devices [19], and Archimedean spirals [20,21]. Among a variety of twisted light types, Laguerre-Gaussian [22,23] and Bessel [24,25] beams are usually distinguished.

For the interaction of a twisted light with matter in the gas phase, both experimental [26] and theoretical researches have been performed for different targets: atoms [27–29], molecules [30,31], and ions [32,33].

The availability of UV twisted radiation makes possible traditional photoelectron spectroscopy, such as the measurements of photoelectron angular distribution (PAD) or spin polarization with twisted radiation. Because the twisting violates the selection rules [34], it may affect photoelectron angular distribution and spin polarization in a very sophisticated way, and the creation of a general theory of photoionization is highly desirable. In Ref. [32] the general formalism of ion photoionization by the twisted Bessel light was developed for the hydrogen-like system with Coulomb wave functions. The photoexcitation of atoms by the Bessel beams has been already discussed in Ref. [35]. Recently, the manifestation of nondipole effects in PADs due to irradiation of atoms by the Bessel light was analyzed in Ref. [36], and the present work is the extension of this approach to other vector correlation parameters of photoionization.

It is reasonable to consider the vector characteristics of a system, such as angular distribution of the reaction products, in terms of a certain spherical harmonic (or Wigner D-function) [37]. Twisted radiation modifies the characteristics, causing redistribution of terms with different ranks. Involving to consideration a particle polarization—either photoelectron or photoion—makes an observable physical picture much more vivid because of a competition between odd and even parameters.

*md.kiselev@physics.msu.ru

Being a fundamental property of particles, spin carries the basis for many processes at different levels of matter, from the bottom with single elementary particles to the top with macroscopic objects. The possibilities of practical applications are quite wide—spintronics, ionic traps, laser cooling, quantum computers [38–43]—and will most likely expand.

Although gaseous targets are the most common species for photoionization experiments, production and detection of spin-polarized electrons emitted in such processes carries difficulties in comparison with the ionization of condensed matter since atoms and molecules in a gas target have predominantly random orientation and the medium itself is sparse.

In conventional photoionization two conditions are necessary for observation of nonzero spin polarization of photoelectrons: (a) the process contains a helix (axial vector) and (b) essential spin-orbit interaction. While the directions of the axial vectors correspond to possible photoelectron spin components, a noticeable spin-orbit interaction makes it possible to resolve spin states of the residual ion or of the electron in continuum.

There are some well-known examples:

(1) *The Fano effect for the spin orientation of the photoelectron ejected by circularly polarized plane-wave light* [44–46]. Electrons are to be collected over the full solid angle of 4π. The helix is provided by the light helicity, and the only possible photoelectron spin component is parallel to the light beam propagation direction. On the contrary, the linearly polarized plane-wave light does not generate the integral spin polarization at all because of lacking the helix.

(2) *Spin polarization observed in angle-resolved experiments on electron emission from unpolarized atoms by the influence of linearly polarized plane-wave light (so-called dynamic polarization)* [47]. Considering the electric dipole approximation, the helix is provided by the vector product of the electric field and the direction of the electron emission, therefore the only allowed spin component is normal to them [48,49].

(3) *Same as (2) but with circularly polarized plane-wave light (so-called polarization transfer)*. In this case an additional helix appears due to the presence of light helicity, and generally speaking all three possible photoelectron spin components could be observed.

It leads to the idea that the introduction of new distinguishable directions into a photoionization process may violate the symmetry of a system and bring new (or change already existing) photoelectron spin components. This direction can be formed by a molecular frame [47], by a strong field [50–54], or by light consisting of components with proportional frequencies [55–57].

In this work we expected to find spectacular manifestation of photoelectron spin polarization during photoionization of atoms by twisted (Bessel) light. In our case the necessary helix is provided by the "twistedness" of light itself. Besides, we have chosen ionization of a krypton $4p$ shell since ionic states $[\mathrm{Ar}]4s^2 4p^{-1}_{3/2}$ and $[\mathrm{Ar}]4s^2 4p^{-1}_{1/2}$ are energetically split quite enough ($\sim$0.67 eV [58]) to be experimentally resolved.

The article is organized as follows. In Sec. II we briefly recall the matrix element evaluation procedure in the case of many-electron atom irradiation by twisted light and construct expressions for photoelectron and photoion statistical tensors in different coordinate systems. In Sec. III we present and discuss results on PADs and spin polarization of photoelectrons ejected by the circularly and linearly polarized Bessel light in $4p$-shell ionization of atomic krypton. Atomic units are used throughout the paper until otherwise specified.

II. GENERAL EQUATIONS

Let us consider an emission of a photoelectron with momentum $\boldsymbol{p}$ and projection of spin onto its propagation direction m_s:

$$\hbar\omega + A(\alpha_i J_i M_i) \to A^+(\alpha_f J_f M_f) + e^-(\boldsymbol{p} m_s), \tag{1}$$

where $A(A^+)$ denotes a state before (after) ionization, i.e., an atom or an ion; $\hbar\omega$ is the photon energy; $J_{i,f}$ and $M_{i,f}$ are the total angular momenta and their projections of the initial and final (atomic and ionic) states; and $\alpha_{i,f}$ are all other quantum numbers needed for the state specification.

A. The twisted-wave matrix element

We chose for analysis photoionization by the Bessel light propagating along the (quantization) z axis. For this case, the Bessel state is characterized by projections of the linear momentum k_z and the total angular momentum (TAM) onto the z axis m_{tam}. The absolute value of the transverse momentum, $\kappa_\perp = |\mathbf{k}_\perp|$, is fixed; together with k_z it defines the energy of the photons $\omega = c\sqrt{\kappa_\perp^2 + k_z^2}$. As shown in Ref. [32], this Bessel state is described by the vector potential

$$\mathbf{A}^{\mathrm{tw}}_{\kappa_\perp m_{\mathrm{tam}}\lambda} = \int \mathbf{u}_\lambda e^{i\mathbf{kr}} a_{\kappa_\perp m_{\mathrm{tam}}}(\mathbf{k}_\perp)\frac{d^2\mathbf{k}_\perp}{4\pi^2}, \tag{2}$$

where

$$a_{\kappa_\perp m_{\mathrm{tam}}}(\mathbf{k}_\perp) = (-i)^{m_{\mathrm{tam}}} e^{i m_{\mathrm{tam}}\phi_k}\sqrt{\frac{2\pi}{k_\perp}}\delta(k_\perp - \kappa_\perp), \tag{3}$$

and $\boldsymbol{u}_\lambda$ is the polarization vector with helicity $\lambda = \pm 1$.

The vector potential of twisted light of any polarization is a combination of the basis components (2) taken with appropriate weights ϵ_λ: $\sum_\lambda \epsilon_\lambda \mathbf{A}^{\mathrm{tw}}_{\kappa_\perp m_{\mathrm{tam}}\lambda}$. For example, "linearly polarized" in the xz plane, Bessel light can be obtained with $\epsilon_{\pm1} = \pm i/\sqrt{2}$ [59]. It should be mentioned that the polarization structure of the twisted beam is a tricky question itself and was a subject of fruitful discussion [60,61].

The Bessel state characterized by Eqs. (2) and (3) can be understood as a coherent superposition of plane waves in momentum space with their wave vectors $\boldsymbol{k} = (\boldsymbol{k}_\perp, k_z)$ lying on the surface of a cone with opening angle $\tan\theta_c = k_\perp/k_z$ (see Fig. 1).

Using the vector potential (2), we obtain the matrix element for photoionization:

$$M^{(\mathrm{tw})}_{M_i\lambda\, m_{\mathrm{tam}} M_f}(\boldsymbol{p}; \theta_c, \boldsymbol{b}_\perp) = \int a_{\kappa_\perp m_{\mathrm{tam}}}(\mathbf{k}_\perp)\, \mathrm{e}^{-i\boldsymbol{k}_\perp \boldsymbol{b}_\perp}\, M^{(\mathrm{pl})}_{M_i\lambda M_f}(\boldsymbol{k}, \boldsymbol{p})\frac{d^2\mathbf{k}_\perp}{4\pi^2}, \tag{4}$$

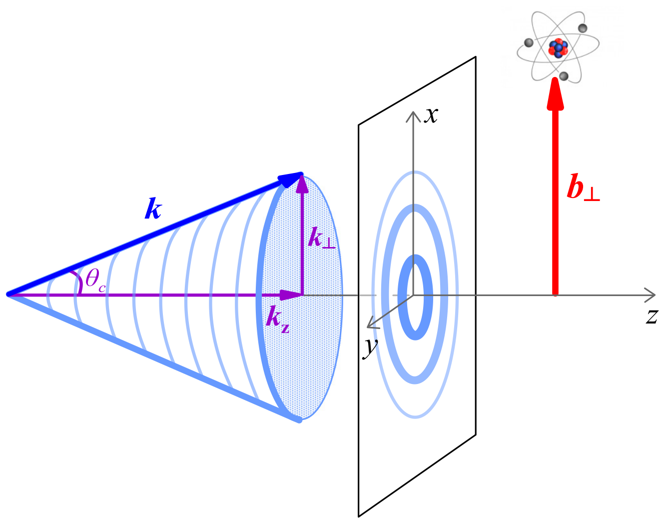

FIG. 1. Overview of the Bessel beam parameters, position of a target atom, and schematic intensity profile in the xy plane.

where $M^{(\mathrm{pl})}_{M_i\lambda M_f}(\boldsymbol{k},\boldsymbol{p})$ is the conventional plane-wave matrix element in the jj-coupling scheme. Therefore,

$$\begin{aligned} M^{(\mathrm{pl})}_{M_i\lambda M_f}(\boldsymbol{k},\boldsymbol{p}) = \sqrt{2\pi} \sum_{LMp} \sum_{\kappa\mu J_t M_t} i^L\,(i\lambda)^p \\ \times \frac{[lL]}{[J_t]}\left(l0,\,\tfrac{1}{2}m_s\,|\,jm_s\right)(J_fM_f,\,j\mu\,|\,J_tM_t) \\ \times (J_iM_i,\,LM\,|\,J_tM_t)\,D^{j*}_{\mu m_s}(\hat{\boldsymbol{p}})\,D^L_{M\lambda}(\hat{\boldsymbol{k}}) \\ \times \langle(\alpha_fJ_f,\epsilon\kappa)J_t||H_\gamma(pL)||\alpha_iJ_i\rangle, \end{aligned} \tag{5}$$

and $D^j_{mm'}(\hat{\boldsymbol{k}})$ is the Wigner D-function (see, for example, Ref. [62]); $\hat{\boldsymbol{k}} = (\phi_k,\theta_k,0)$ defines the direction of the incident (plane-wave) photon; $\hat{\boldsymbol{p}} = (\phi_p,\theta_p,0)$ is the propagation direction of the photoelectron; and $\kappa = j + 1/2$ for $l = j \pm 1/2$ (l is the orbital angular momentum of the electron) defines the Dirac angular-momentum quantum number. Note that projection of total photoelectron momentum μ and the whole system momentum M_t are in the laboratory coordinate system. The notation $[abc...] \equiv \sqrt{(2a+1)(2b+1)(2c+1)...}$ and standard designation for the Clebsch-Gordan coefficients are used. Operator $H_\gamma(pL)$ is responsible for the interaction between the atomic electron and magnetic ($p=0$) or electric ($p=1$) photon with multipolarity L. Note that the reduced matrix element $\langle(\alpha_fJ_f,\epsilon\kappa)J_t||H_\gamma(pL)||\alpha_iJ_i\rangle$ includes the scattering phase dependence (see Ref. [36] for details). In Eq. (4) the factor $\mathrm{e}^{-i\boldsymbol{k}_\perp\boldsymbol{b}_\perp}$ with $\boldsymbol{b}_\perp = (b_x, b_y)$ specifies the position of the target atom regarding the quantization axis of the incident light (see Fig. 1).

Applying two vector potentials (2) obtained for different TAM projections and different helicities, one can derive the matrix element of photoionization by twisted light of any polarization:

$$M^{(\mathrm{tw})}_{M_iM_f}(\boldsymbol{p};\theta_c,\,\boldsymbol{b}_\perp) = \sum_\lambda \epsilon_\lambda\,M^{(\mathrm{tw})}_{M_i\lambda\,m_{\mathrm{tam}}=m+\lambda\,M_f}(\boldsymbol{p};\theta_c,\,\boldsymbol{b}_\perp), \tag{6}$$

in terms of the matrix elements (4).

B. Observable parameters

We consider the target (atom) to be initially unpolarized and distinguish cases when polarization of the photoelectron and photoion is detected. Therefore, we average the photoemission probability over initial magnetic quantum number M_i and sum incoherently either over final magnetic quantum number M_f or m_s. Evaluation of the angle-resolved spin polarization of a macroscopic (i.e., consists of atoms randomly and uniformly distributed within the xy plane) atomic target can be performed by averaging the product of matrix elements corresponding to specific quantum numbers of electron spin projection m_s, m_s' (4) over the impact parameter:

$$\begin{aligned} \frac{\mathrm{d}\sigma^{(\mathrm{tw})}_{m_sm_s'}}{\mathrm{d}\Omega_p}(\theta_p,\phi_p;\,\theta_c) &= \mathcal{N}\frac{1}{2J_i+1}\sum_{M_iM_f}\sum_{\lambda,\lambda'}\epsilon_\lambda\epsilon^*_{\lambda'}\int M^{(\mathrm{tw})}_{M_i\lambda\,m_{\mathrm{tam}}=m+\lambda\,M_f}(\boldsymbol{p};\theta_c,\,\boldsymbol{b}_\perp)\,M^{(\mathrm{tw})*}_{M_i\lambda'\,m_{\mathrm{tam}}=m+\lambda'\,M_f}(\boldsymbol{p};\theta_c,\,\boldsymbol{b}_\perp)\,\frac{d\boldsymbol{b}_\perp}{\pi R^2} \\ &= \mathcal{N}\frac{1}{2J_i+1}\sum_{M_iM_f}\sum_{\lambda,\lambda'}\epsilon_\lambda\epsilon^*_{\lambda'}\int M^{(\mathrm{pl})}_{M_i\,\lambda\,M_f}(\boldsymbol{k},\boldsymbol{p})\,M^{(\mathrm{pl})*}_{M_i\,\lambda'\,M_f}(\boldsymbol{k},\boldsymbol{p})\,\mathrm{e}^{i(\lambda-\lambda')\phi_k}\,\frac{d\phi_k}{2\pi}, \end{aligned} \tag{7}$$

where the parameter R defines the "size" of a target and is assumed to be much larger than the characteristic size of the Bessel beam intensity profile patterns. The evaluation of the prefactor $\mathcal{N}$ requires redefinition of the concept of cross section [63] and is not a subject of the current investigation, because here we are interested in the nondimensional parameters.

To simplify Eq. (7), we first substitute the matrix elements (5) and obtain integral

$$\int d\phi_k\,e^{i(\lambda-\lambda')\phi_k}D^s_{\lambda-\lambda',\,q}(\hat{\boldsymbol{k}}^{-1}) = 2\pi\,d^s_{qq}(\theta_c)\delta_{q,\,\lambda-\lambda'}, \tag{8}$$

where $\hat{\boldsymbol{k}}^{-1} \equiv (0,\theta_c,\phi_k)$ and $d^j_{mm'}(\theta_c)$ is small Wigner D-function (see, for example, Ref. [62]).

One can see that parameter $\boldsymbol{b}_\perp$, which may be essential to account for a complex internal structure of a twisted light consisting of concentric rings of high and low intensity, is smeared out for a macroscopic target.

In this way we obtain the expression for the component of the angle-resolved spin density matrix elements:

$$\begin{aligned} \frac{\mathrm{d}\sigma^{(\mathrm{tw})}_{m_s,m_s'}}{\mathrm{d}\Omega_p}(\theta_p,\phi_p;\,\theta_c) = \frac{2\pi\mathcal{N}}{2J_i+1}\sum_{k,q,k_l}D^{k*}_{q\,q_s}(\phi_p,\theta_p,0)\,d^k_{qq}(\theta_c)\sum_{LL'pp'}(-1)^{1/2-m_s'}\delta_{q,\xi}\,\rho_{k\xi}[pL,\,p'L'] \\ \times (1/2\,m_s,\,1/2-m_s'\,|\,k_sq_s)(k_l0,\,k_sq_s\,|\,kq_s)B^{pL,p'L'}[k_l,k_s,k], \end{aligned} \tag{9}$$

where the dynamical parameter

$$B^{pL,p'L'}[k_l,k_s,k]=\sum_{\kappa\kappa' J_t J_t'}(-1)^{J_i-J_f+L'-j'+l'}[ll'jj'LL'J_tJ_t'k_lk_s](l0,l'0\,|\,k_l0)\begin{Bmatrix} l & 1/2 & j\\ l' & 1/2 & j'\\ k_l & k_s & k\end{Bmatrix}$$
$$\times\begin{Bmatrix} J_t & J_t' & k\\ L' & L & J_i\end{Bmatrix}\begin{Bmatrix} J_t & J_t' & k\\ j' & j & J_f\end{Bmatrix}\langle(\alpha_fJ_f,\epsilon\kappa)J_t||H_\gamma(pL)||\alpha_iJ_i\rangle\,\langle(\alpha_fJ_f,\epsilon\kappa')J_t'||H_\gamma(p'L')||\alpha_iJ_i\rangle^* \qquad (10)$$

does not depend on the polarization parameters and remains the same in any coordinate system, and

$$\rho_{k\xi}[pL,p'L']=\sum_{\lambda\lambda'}\epsilon_\lambda\epsilon^*_{\lambda'}i^{L-L'}(i\lambda)^p(-i\lambda')^{p'}(-1)^{L'+\lambda'}(L\lambda,L'-\lambda'\,|\,k\xi) \qquad (11)$$

is the statistical tensor of the photon with definite multipolarity and type. Remember the general connection between density matrix $\rho(am_a,a'm_a')$ and statistical tensor $\rho_{kq}[a,a']$ of the same momentum a: $\rho_{kq}[a,a']=\sum(-1)^{a'-m_a'}(am_a,a'-m_a'\,|\,kq)\rho(am_a,a'm_a')$. Therefore, the photoelectron statistical tensor as a function of $(\theta_p,\phi_p;\theta_c)$ is

$$\rho^{(\mathrm{tw})}_{k_sq_s}[1/2,1/2]=\sum_{kq}D^{k*}_{q\,q_s}(\phi_p,\theta_p,0)\,d^k_{qq}(\theta_c)\sum_{LL'pp'}\rho_{kq}[pL,p'L'](k_l0,k_sq_s\,|\,kq_s)B^{pL,p'L'}[k_l,k_s,k]. \qquad (12)$$

In Eq. (10) and below, constructions in curly brackets are standard notations for $6j$ and $9j$ symbols.

For constructions (11) the usual tensor's permutation rule is fair: $\rho_{k\xi}[pL,p'L']=(-1)^{L-L'+\xi}\rho^*_{k-\xi}[p'L',pL]$. Additionally, for the dynamical parameters (10), $B^{Lp,L'p'}[k_l,k_s,k]=(-1)^{k_l+k_s+k+L-L'}B^{L'p',Lp}[k_l,k_s,k]^*$. The permutation connection for (12) is $\rho^{(\mathrm{tw})}_{k_sq_s}[1/2,1/2]=(-1)^{q_s}\rho^{(\mathrm{tw})*}_{k_s-q_s}[1/2,1/2]$. If one puts $k_s=0$, $q_s=0$ into (12), the equation turns to the PAD and coincides with Eqs. (19) or (27) from Ref. [36] up to normalization. Since we are interested in dimensionless parameters of angular anisotropy and spin polarization, we do not normalize the density matrix and its trace is proportional to ionization probability. The form of Eqs. (9) and (12) is convenient because it clearly separates the dynamical factor (10) depending on target details (atom, ionizing shell, photon energy, etc.) from the kinematic (geometrical) factor (11) depending on polarization, orientation, and others.

Following a similar way with a minor difference in summing over m_s instead of M_f and integrating over the electron emission angle, one may easily obtain the statistical tensor components for the residual ion:

$$\bar\rho^{(\mathrm{tw})}_{k_fq_f}[J_f,J_f]=\delta_{kk_f}\delta_{qq_f}d^k_{qq}(\theta_c)\sum_{LL'pp'}\rho_{kq}[pL,p'L']\bar B^{pL,p'L'}[k] \qquad (13)$$

with the dynamical parameter

$$\bar B^{pL,p'L'}[k]=\sum_{\kappa\kappa' J_tJ_t'}(-1)^{J_i+J+L'-J_f-j-J'}[LL'J_tJ_t']\begin{Bmatrix} J_t & J_t' & k\\ L' & L & J_i\end{Bmatrix}\begin{Bmatrix} J_t & J_t' & k\\ J_f & J_f & j\end{Bmatrix}$$
$$\times\ \langle(\alpha_fJ_f,\epsilon\kappa)J_t||H_\gamma(pL)||\alpha_iJ_i\rangle\,\langle(\alpha_fJ_f,\epsilon\kappa')J_t'||H_\gamma(p'L')||\alpha_iJ_i\rangle^*. \qquad (14)$$

The ratios of the components (13) define polarization (orientation and alignment) of the ion.

The Cartesian components of electron spin polarization are related to the statistical tensors in the same coordinate system:

$$S_z=\frac{\rho_{10}[1/2,1/2]}{\rho_{00}[1/2,1/2]}, \qquad (15)$$

$$S_x=-i\,\frac{\rho_{11}[1/2,1/2]+\rho_{1-1}[1/2,1/2]}{\sqrt2\rho_{00}[1/2,1/2]}, \qquad (16)$$

$$S_y=-\frac{\rho_{11}[1/2,1/2]-\rho_{1-1}[1/2,1/2]}{\sqrt2\rho_{00}[1/2,1/2]}, \qquad (17)$$

and PAD is defined by

$$W=\sqrt2\rho_{00}[1/2,1/2]. \qquad (18)$$

For the coordinate system used in (12) the z component is along the photoelectron emission direction, the x component is in the plane formed by the direction of electromagnetic field propagation and of electron emission (*tangential* component), and the y component is orthogonal to these vectors (*normal* component) (see coordinate systems marked by red in Figs. 2 and 3).

In dipole approximation the explicit forms of Eqs. (12) are

$$\rho^{(\mathrm{tw})}_{00}=\rho^{E1}_{00}B[0,0,0]+\sum_q D^{2*}_{q0}(\phi_p,\theta_p,0)\,d^2_{qq}(\theta_c)\rho^{E1}_{2q}B[2,0,2] \qquad (19)$$

$$\rho^{(\mathrm{tw})}_{10}=\sum_q D^{1*}_{q0}(\phi_p,\theta_p,0)\,d^1_{qq}(\theta_c)\rho^{E1}_{1q}B[0,1,1]-\sqrt{\frac25}D^{1*}_{q0}(\phi_p,\theta_p,0)\,d^1_{qq}(\theta_c)\rho^{E1}_{1q}B[2,1,1] \qquad (20)$$

$$\rho^{(\mathrm{tw})}_{11}=\sum_q D^{1*}_{q1}(\phi_p,\theta_p,0)\,d^1_{qq}(\theta_c)\rho^{E1}_{1q}B[0,1,1]+\frac{1}{\sqrt{10}}D^{1*}_{q1}(\phi_p,\theta_p,0)\,d^1_{qq}(\theta_c)\rho^{E1}_{1q}B[2,1,1]-\frac{1}{\sqrt2}D^{2*}_{q1}(\phi_p,\theta_p,0)\,d^2_{qq}(\theta_c)\rho^{E1}_{2q}B[2,1,2]. \qquad (21)$$

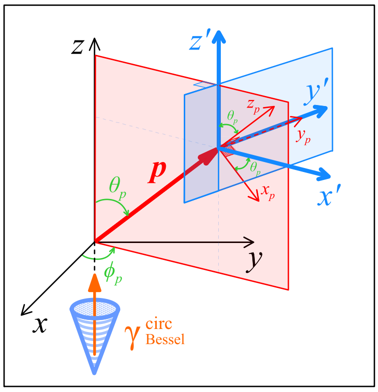

FIG. 2. Coordinate systems used in analysis of ionization by circularly polarized Bessel beam: laboratory coordinate system $S(x, y, z)$; photoelectron coordinate system $S_p(x_p, y_p, z_p)$, in which statistical tensors (22)–(24) are written; and coordinate system $S'(x', y', z')$ obtained from S_p after the Euler's angles rotation $\omega_{\text{circ}} = \{0; -\theta_p; 0\}$, in which statistical tensors (29)–(31) are written.

Here and below, for brevity we put $B^{E1,E1}[k_l, k_s, k] \equiv B[k_l, k_s, k]$, $\rho^{(\text{tw})}_{kq}[1/2, 1/2] \equiv \rho^{(\text{tw})}_{kq}$ and $\rho_{kq}[E1, E1] \equiv \rho^{E1}_{kq}$. According to the permutation rules for dynamical parameters, it is obvious that $B[0, 0, 0]$, $B[2, 0, 2]$, $B[0, 1, 1]$, and $B[2, 1, 1]$ have only real parts, but $B[2, 1, 2]$ is completely imaginary.

For the circularly polarized beam $\epsilon_{\pm 1} = 1$, $\rho^{E1}_{00} = 1/\sqrt{3}$, $\rho^{E1}_{10} = \pm 1/\sqrt{2}$ (responsible for transfer of polarization), $\rho^{E1}_{20} = 1/\sqrt{6}$, and thus

$$\rho^{(\text{tw})}_{00} = \frac{1}{\sqrt{3}} B[0, 0, 0] + \frac{1}{\sqrt{6}} P_2(\cos\theta_p)\, P_2(\cos\theta_c) B[2, 0, 2] \tag{22}$$

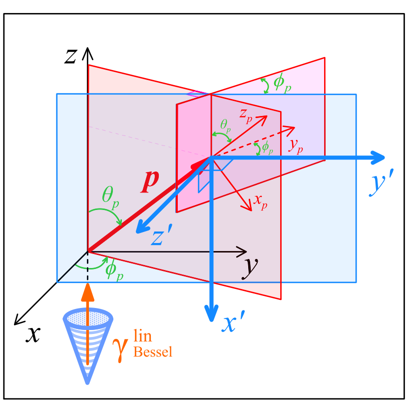

FIG. 3. Coordinate systems used in analysis of ionization by linearly polarized Bessel beam: laboratory coordinate system $S(x, y, z)$; photoelectron coordinate system $S_p(x_p, y_p, z_p)$, in which statistical tensors (32) and (33) are written; coordinate system $S'(x', y', z')$ obtained from S_p after two subsequent Euler's angles rotations: $\omega^{(1)}_{\text{lin}} = \{0; -\theta_p; -\phi_p\}$ and $\omega^{(2)}_{\text{lin}} = \{0; \pi/2; 0\}$, in which statistical tensors (36)–(38) are written.

$$\rho^{(\text{tw})}_{10} = \frac{\pm 1}{\sqrt{2}} \cos\theta_p \cos\theta_c \left(B[0, 1, 1] - \sqrt{\frac{2}{5}} B[2, 1, 1] \right) \tag{23}$$

$$\begin{aligned}\rho^{(\text{tw})}_{11} = -\frac{1}{2} \sin\theta_p \Bigg\{ &\mp \cos\theta_c \left(B[0, 1, 1] + \frac{1}{\sqrt{10}} B[2, 1, 1] \right) \\ &+ \frac{1}{\sqrt{2}} \cos\theta_p\, P_2(\cos\theta_c) B[2, 1, 2] \Bigg\},\end{aligned} \tag{24}$$

where $P_n(x)$ is the Legendre polynomial of the n-th order.

Similar to the case of plane-wave ionization, Eqs. (22)–(24) possess axial symmetry with respect to the beam propagation direction. No additional spin component appears, but the dependency of them on the opening angle θ_c is different. For example, the imaginary part of Eq. (24) turns to zero at $\theta_c = \arccos(1/\sqrt{3})$, while the real part is conserved and the electron is polarized in the xz plane.

The orientation and alignment of the residual ion for twisted and plane radiation are connected as

$$\mathcal{A}^{(\text{tw})}_{10} = \frac{\bar{\rho}^{(\text{tw})}_{10}[J_f, J_f]}{\bar{\rho}^{(\text{tw})}_{00}[J_f, J_f]} = \cos\theta_c\, \mathcal{A}_{10}\,; \tag{25}$$

$$\mathcal{A}^{(\text{tw})}_{20} = \frac{\bar{\rho}^{(\text{tw})}_{20}[J_f, J_f]}{\bar{\rho}^{(\text{tw})}_{00}[J_f, J_f]} = \left(\frac{3\cos^2\theta_c - 1}{2} \right) \mathcal{A}_{20}. \tag{26}$$

Therefore, the orientation drops with cone angle slower than the alignment. Remember a presentation of polarization in terms of population n_{M_f} of sublevels with definite magnetic quantum number M_f:

$$\mathcal{A}_{k0} = [J_f] \frac{\sum_{M_f} (-1)^{J_f - M_f} (J_f M_f, J_f - M_f \,|\, k0) n_{M_f}}{\sum_{M_f} n_{M_f}}. \tag{27}$$

Therefore, Eqs. (25) and (26) may be understood as averaged over a macroscopic target population of different magnetic sublevels.

Statistical tensors under the Euler angles' rotation $\omega = \{\alpha; \beta; \gamma\}$ transforms as [62]

$$\widetilde{\rho}_{k'q'}[j, j'] = \delta_{kk'} \sum_q \rho_{kq}[j, j'] D^{k*}_{qq'}(\omega). \tag{28}$$

In order to discuss the case of photoionization by a circularly polarized Bessel beam in the laboratory coordinate system, it is sufficient to transform the photoelectron coordinate system $S_p(x_p, y_p, z_p)$ into the system $S'(x', y', z')$ in such a way that the z' axis aligns with the z axis. That could be done by Euler's rotation $\omega_{\rm circ} = \{0; -\theta_p; 0\}$ (see Fig. 2), and then the statistical tensors' components in the case of circular polarization become

$$\widetilde{\rho}_{00}^{\,(\rm tw)} = \rho_{00}^{(\rm tw)} \tag{29}$$

$$\widetilde{\rho}_{10}^{\,(\rm tw)} = \sqrt{2}\sin\theta_p\,{\rm Re}\rho_{11}^{(\rm tw)} + \rho_{10}^{(\rm tw)}\cos\theta_p = \pm\frac{\cos\theta_c}{\sqrt{2}}\left(B[0,1,1] - \sqrt{\frac{2}{5}}B[2,1,1]P_2(\cos\theta_p)\right) \tag{30}$$

$$\widetilde{\rho}_{11}^{\,(\rm tw)} = \cos\theta_p\,{\rm Re}\rho_{11}^{(\rm tw)} - \frac{\sin\theta_p}{\sqrt{2}}\rho_{10}^{(\rm tw)} + i\,{\rm Im}\rho_{11}^{(\rm tw)} = \pm\frac{\sin\theta_p\cos\theta_p}{2\sqrt{2}}\left(\frac{3}{\sqrt{5}}\cos\theta_c B[2,1,1] \mp i\,P_2(\cos\theta_c){\rm Im}B[2,1,2]\right). \tag{31}$$

The part of (30) without angle dependency on θ_p is the only component which is conserved at integration over the photoemission direction, which is very similar to the Fano effect [44–46] in the case of ionization by the plane-wave beam. The second term of (30) provides the angular dependency of the spin component oriented along the beam propagation direction. The form of (31) allows for clearly distinguishing the real part, responsible for the spin component in the plane of electron emission, and the imaginary part, responsible for the component orthogonal to it.

For the light linearly polarized along the x axis $\epsilon_{\pm1} = \pm i/\sqrt{2}$, $\rho_{00}^{E1} = 1/\sqrt{3}$, $\rho_{20}^{E1} = 1/\sqrt{6}$, $\rho_{2\pm2}^{E1} = -1/2$, and thus

$$\begin{aligned}\rho_{00}^{(\rm tw)} = {}& \frac{1}{\sqrt{3}}B\,[0,0,0] + \frac{1}{\sqrt{6}}B\,[2,0,2]\bigg\{1 - 3\sin^2\theta_p\cos^2\phi_p - 6\sin^2(\theta_c/2)(\cos^2\theta_p - \sin^2\theta_p\cos^2\phi_p)\\ &+ \frac{3}{2}\sin^4(\theta_c/2)(5\cos^2\theta_p - 1 - 2\sin^2\theta_p\cos^2\phi_p)\bigg\}\end{aligned} \tag{32}$$

$$\begin{aligned}\rho_{11}^{(\rm tw)} = {}& -\frac{1}{\sqrt{2}}B\,[2,1,2]\sin\theta_p\bigg\{\cos\theta_p\cos^2\phi_p + i\cos\phi_p\sin\phi_p - 2\sin^2(\theta_c/2)(\cos\theta_p(1+\cos^2\phi_p) + i\cos\phi_p\sin\phi_p)\\ &+ \sin^4(\theta_c/2)\left(\cos\theta_p\left(\frac{5}{2} + \cos^2\phi_p\right) + i\cos\phi_p\sin\phi_p\right)\bigg\}.\end{aligned} \tag{33}$$

Note that because statistical tensors ρ_{1q} are forbidden for linear polarization, there is no transfer polarization in this case.

The ratio $-\sqrt{2}B[2,0,2]/B[0,0,0]$ at $\theta_c = 0$ is the conventional angular anisotropy parameter β of PAD. Three important notes should be mentioned: (1) there is no tensor component with $q_s = 0$, which means that there is no spin component oriented along the photoelectron emission direction, as it is for plane-wave ionization [49,64]; (2) accounting for the fact that $B[2,1,2]$ is imaginary, the coordinates $n'_x = \{\sin\theta_p\cos\phi_p, \sin\theta_p\sin\phi_p, \cos\theta_p\}$, $n'_y = \{-\sin\phi_p, \cos\phi_p, 0\}$, and substituting $\theta_c = 0$ into Eq. (33), one can check that there is no spin component oriented along the polarization vector in the case of plane-wave ionization [49,64]; and (3) since real and imaginary parts of Eq. (33) depend on the opening angle θ_c in a different way, an additional spin component oriented along the linear polarization vector appears for the twisted light.

For the linearly polarized twisted light there are only second-rank components of the polarization:

$$\mathcal{A}_{20}^{(\rm tw)} = \left(\frac{3\cos^2\theta_c - 1}{2}\right)\mathcal{A}_{20}\,; \tag{34}$$

$$\mathcal{A}_{2\pm2}^{(\rm tw)} = \cos^4(\theta_c/2)\,\mathcal{A}_{2\pm2}. \tag{35}$$

As it is for circularly polarized light, the dependency of different components of polarization on the cone angle is different.

In order to look carefully at the component of photoelectron spin polarization oriented along the polarization, it is constructive to switch into the system where new axis z' is along the polarization vector (original x axis). The corresponding rotation is performed using Eq. (28) via two subsequent rotations: $\omega_{\rm lin}^{(1)} = \{0; -\theta_p; -\phi_p\}$ and $\omega_{\rm lin}^{(2)} = \{0; \pi/2; 0\}$ (see Fig. 3). After that transformation, the statistical tensors' components become

$$\widetilde{\rho}_{00}^{\,(\rm tw)} = \rho_{00}^{(\rm tw)} \tag{36}$$

$$\widetilde{\rho}_{10}^{\,(\rm tw)} = -\sqrt{2}\left(\cos\theta_p\cos\phi_p\,{\rm Re}\rho_{11}^{(\rm tw)} + \sin\phi_p\,{\rm Im}\rho_{11}^{(\rm tw)}\right) = \frac{\cos\theta_p\sin\theta_p\sin\phi_p}{2}{\rm Im}B[2,1,2]\sin^2\frac{\theta_c}{2}\left(5\sin^2\frac{\theta_c}{2} - 4\right) \tag{37}$$

$$\begin{aligned}\widetilde{\rho}_{11}^{(\mathrm{tw})} &= \sin\theta_p\,\mathrm{Re}\rho_{11}^{(\mathrm{tw})} + i\big(\cos\phi_p\,\mathrm{Im}\rho_{11}^{(\mathrm{tw})} - \sin\phi_p\cos\theta_p\,\mathrm{Re}\rho_{11}^{(\mathrm{tw})}\big)\\ &= \frac{\sin\theta_p\cos\phi_p}{\sqrt{2}}\mathrm{Im}B[2,1,2]\left\{\sin\theta_p\sin\phi_p\cos^4\frac{\theta_c}{2} - i\cos\theta_p\left(1-4\sin^2\frac{\theta_c}{2}+\frac{7}{2}\sin^4\frac{\theta_c}{2}\right)\right\}.\end{aligned} \tag{38}$$

All spin components arising for the linearly polarized twisted beam are determined by the only dynamical parameter $B[2, 1, 2]$. The component (37) arises only for twisted radiation and does not exist for plane radiation.

While the physical meaning of a photoelectron spin is unambiguous, the orientation and alignment need additional discussion for the macroscopic targets. The ionic polarization parameters may be interpreted in the same way as for the electron: assuming that a detector registers ions in the state with particular projection M_f to a quantization axis and casting an appropriate combination (27). On the other hand, in reality, an ionic polarization is detected via some subsequent process. Our analysis has shown that if this subsequent process applying to determine the polarization does not involve the twisted light (for example, Auger decay or fluorescence), then the target averaged parameters (25), (26), (34), and (35) may be used in the usual way. However, if the process applied to determine polarization involves the twisted light (for example, subsequent ionization of the ion or laser-assisted Auger decay), then the equation becomes inapplicable.

III. RESULTS AND DISCUSSION

To illustrate the effects of twisting inprinted into a vector correlation, i.e., photoelectron angular distribution and spin polarization, we consider valence $4p$-shell ionization of krypton in the energy range below 90 eV not reaching the $3d$-shell ionization thresholds [58]. The initial state of neutral krypton was prepared using the multiconfiguration Hartree-Fock method as a pure $[\mathrm{Ar}]4s^24p^6\,{}^1S_0$ state by means of MCHF code [65]. After that, the [Ar] core was frozen and used to obtain $4s$ and $4p$ orbitals of final ionic state $[\mathrm{Ar}]4s^24p^5$, optimizing them on the ${}^2P$ term. The subsequent Breit-Pauli diagonalization procedure [66] was used in order to construct j-split states $[\mathrm{Ar}]4s^24p^5\,{}^2P_{3/2,\,1/2}$. After that, we applied the B-spline R-matrix approach [67] to calculate photoionization amplitudes of the process (1) with the use of measured $4p_{3/2,1/2}$ subshell ionization thresholds [58]. The quality of the model is sufficient to describe reasonably the behavior of the dipole anisotropy parameter β of the PAD due to krypton $4p$-shell photoionization (see Fig. 4). The model predicts the dipole Cooper minimum at ∼82 eV, which is close enough to the more precise calculations of Ref. [68].

In Fig. 5 we present the ratio of the dynamical parameters (10) to zero-rank $B[0, 0, 0]$, because specifically these parameters determine the vector correlation characteristics. Quite typically, the dipole angular anisotropy parameter $\beta \sim B[2, 0, 2]/B[0, 0, 0]$ behaves in the same way for ionization into the $J_f = 3/2$ and $J_f = 1/2$ final ionic state (blue line in Figs. 5(a) and 5(b)), while spin polarization proportional to $B[k_l, 1, k]/B[0, 0, 0]$ possesses an opposite sign and approximately twice smaller value for $J_f = 3/2$ [70]. The component $B[k = \{0, 2\}, 1, 1]/B[0, 0, 0]$ is formed by

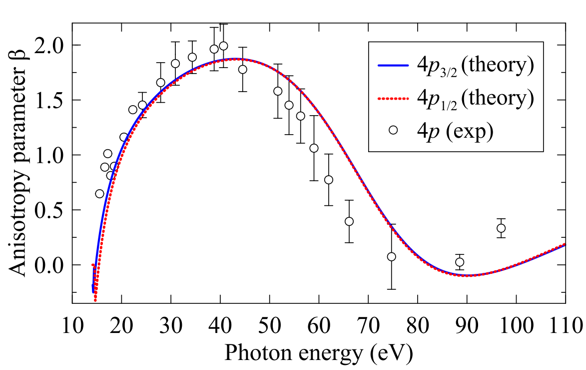

FIG. 4. Simulated according to the present theoretical model (see text), anisotropy parameter β for the PAD due to photoionization of a krypton atom for final ionic states Kr^+4p^5 with $J_f = 3/2$ (solid blue line) and $J_f = 1/2$ (dotted red line). Experimental data are taken from Ref. [69].

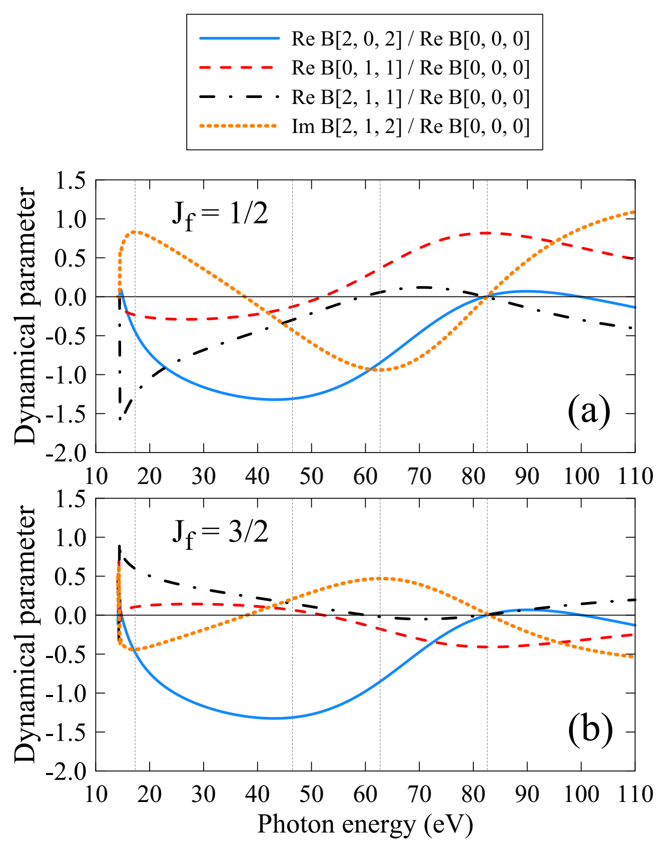

FIG. 5. Photon energy dependencies of the dynamical parameters relative to the value of $B[0, 0, 0]$ for final ionic states of $\mathrm{Kr}^+\,4p^5$ with $J_f = 1/2$ (a) and $J_f = 3/2$ (b). Vertical dashed gray lines correspond to photon energies selected for analysis (see text).

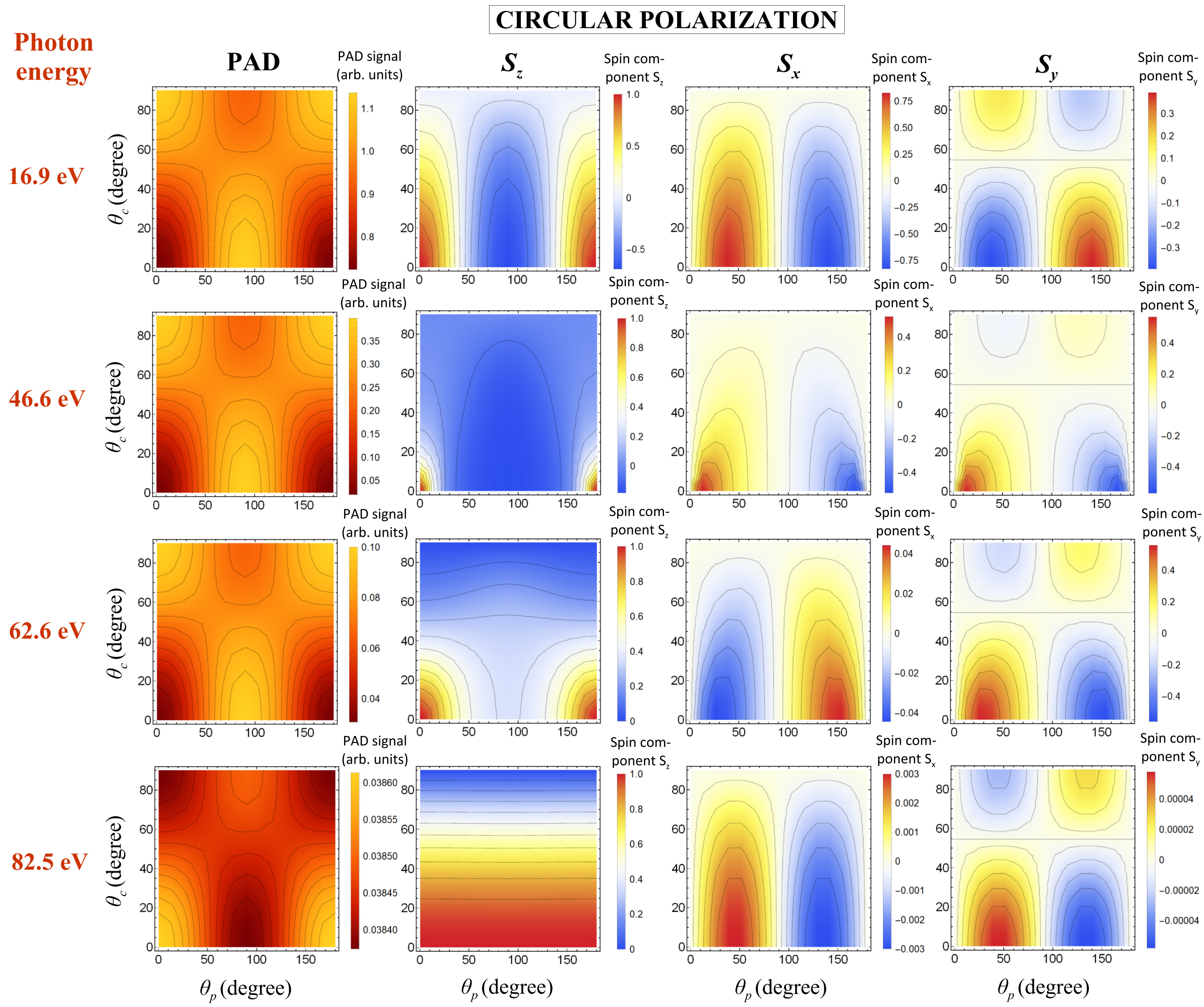

FIG. 6. PAD (first column) and photoelectron spin component along the field propagation direction S_z (second column), in the direction of electron momentum projection to the xy plane S_x (third column) and in the direction perpendicular to field propagation and electron momentum S_y (fourth column) as a function of polar emission angle θ_p and cone angle θ_c in the case of krypton atom ionization by circularly polarized Bessel light.

transfer of polarization in terms of Ref. [47], and appears due to the circularly polarized component of the radiation. The component $B[2, 1, 2]/B[0, 0, 0]$ is *dynamical polarization*, and appears due to fine-structure splitting. It has been the subject of a number of investigations that typically dynamical polarization is smaller than polarization transfer [64,71–76]. The component $B[0, 1, 1]/B[0, 0, 0]$ (red dashed line in Fig. 5) is the only one which is conserved after integration over the photoelectron emission angle and therefore for the detectors which collect all of the electrons. There is a Cooper minimum in the $\varepsilon d\ j$ ionization amplitude near 80 eV which governs the zero of $B[2, k_s, k]/B[0, 0, 0]$ (blue, orange, and black lines in Figs. 5(a) and 5(b)). In the opposite, the component $B[0, 1, 1]/B[0, 0, 0]$ which contains $\varepsilon s\,1/2$ amplitude manifests a maximum at this energy. One can see that $B[2, 0, 2]/B[0, 0, 0]$ in Fig. 5 approaches very close to the minimal possible value $-\sqrt{2}$ at energy 40 eV. To reach this value, the ratio of $\varepsilon s\,1/2$ and $\varepsilon d\,3/2$ amplitudes should be real and equal $1/\sqrt{2}$ (for $J_f = 1/2$) and $-\sqrt{5}$ (for $J_f = 3/2$). Substituting this ratio into Eqs. (10), one gets zero for all of the spin components. Therefore, the crossing of all curves near 40 eV is not occasional. For $J_f = 3/2$ (Fig. 5(b)) there are two $\varepsilon d\,3/2(5/2)$ amplitudes, and the explanation is a bit trickier but still fair. To apply the same discussion, we need to assume weak dependency of continuum wave function on quantum number j. Then, the ratio of ionization amplitudes into $d5/2$ and $d3/2$ tends to 3.

In Fig. 6 the PAD and spin components due to ionization of krypton by the circularly polarized Bessel light are presented as a function of the polar emission angle θ_p and cone angle θ_c for different photon energies marked in Fig. 5 by the vertical lines. Presented results are calculated for residual ions in the state $J_f = 1/2$, and the results for $J_f = 3/2$ are easily deduced by comparison of Figs. 5(a) and 5(b).

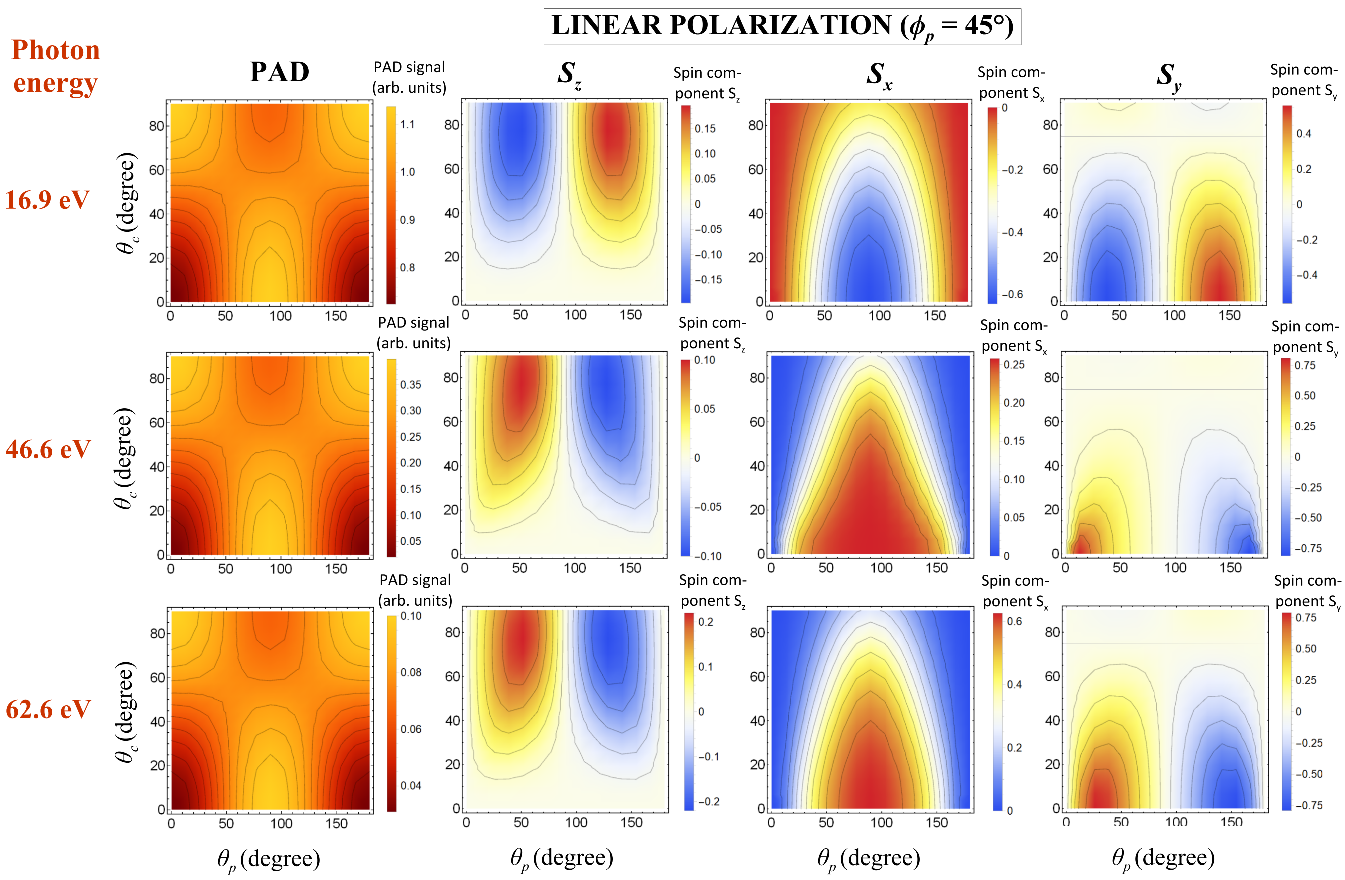

FIG. 7. PAD (first column) and photoelectron spin component along the field polarization S_z (second column), in the field propagation direction S_x (third column), and in the direction perpendicular to them S_y (fourth column) as a function of polar emission angle θ_p and cone angle θ_c in the case of krypton atom ionization by linearly polarized Bessel light. The angle $\phi_p = 45^\circ$.

The probability of electron emission (Fig. 6, first column) caused by plane-wave light (θ_c tends to zero) is maximal in the plane perpendicular to the propagation direction, but the maximum turns to minimum when the cone angle increases. For the photon energy 82.5 eV, the PAD is practically uniform because $\beta \approx 0$. The component parallel to the field propagation direction S_z (second column) may form a quite complicated pattern if $B[2, 1, 1]/B[0, 0, 0]$ is essential: for this target ($4p$ shell of krypton) it corresponds to low energy 16.9 eV (see Fig. 6, upper row). When the ratio $B[2, 1, 1]/B[0, 0, 0]$ drops, the angular pattern becomes more uniform and the minima at $\theta_p = 90^\circ$ completely disappears at 82.5 eV. Thus, the zero spin at $\theta_p = 45^\circ$ for low energy (second column, first row) is dynamical and depends on the ionization amplitudes. Two other components lie on the plane perpendicular to the field propagation direction: S_x (third column) is parallel to the projection of electron momentum to this plane, and S_y (fourth column) is orthogonal. Both possess a maximum at $\theta_p = 45^\circ$ according to Eq. (24). Remarkably, while S_z and S_x decrease with cone angle, the S_y component has a more complicated pattern with a zero point at $\cos\theta_c = 1/\sqrt{3}$ (marked by the horizontal line), and for the cone angle above this value the spin changes orientation.

In Fig. 7 the PAD and spin components due to ionization of krypton by the linearly polarized Bessel light are presented as a function of polar emission angle θ_p and cone angle θ_c at the fixed azimuth angle $\phi_p = 45^\circ$ for different photon energies marked in Fig. 5 by the vertical lines (for residual ion in the state $J_f = 1/2$). Since the photoemission is caused by linearly polarized radiation, the transfer mechanism does not contribute and the attitude of spin polarization is lower than in the case of circularly polarized radiation. In ionization by plane-wave linearly polarized radiation, spin polarization cannot be oriented either along the polarization vector or along electron emission. The last component does not appear for the twisted radiation either [see Eq. (33)]. Remarkably, spin orientation along polarization is allowed and increases with cone angle θ_c (see Fig. 7, second column). The other two component $S_{x,y}$ behave in a different way as a function of the cone angle. Besides, S_y manifests a zero at $\sin^2(\theta_c/2) = (4 - \sqrt{2})/7$ and changes orientation after that. It is also interesting to note that PAD defined by Eq. (18) in the case of the linearly polarized Bessel beam coincides exactly with that of the circularly polarized Bessel beam at $\phi_p = 45^\circ$ (see first columns of Figs. 6 and 7). That directly (but not quite evidently at the same time) follows from the comparison of Eqs. (22) and (32).

IV. CONCLUSIONS

In the current work we present an investigation of photoelectron and photoion polarization in an ionization caused by the twisted Bessel light. More precisely, we obtain the equations for electron spin polarization, ionic orientation, and alignment in terms of photoionization amplitudes within a jj-coupling scheme in general form and in the dipole approximation. The equations are applicable for the extended target with uniform distribution of atoms. The photoelectron spin is considered in two coordinate systems related to photoelectron emission and the beam propagation direction. That allows us to analyze in great detail dependencies on the twisted light cone angle.

As for plane-wave radiation, in the case of the circularly polarized beam there is a spin component oriented along the beam propagation direction which is conserved after integration over the photoemission direction. In the case of twisted radiation, the angular dependency of this component is dynamically connected with the cone angle. We show that the lowest ranked polarization parameter, e.g., ion orientation, and the components coplanar to the beam propagation and emission directions (conserved part of S_z and tangential components) monotonically decrease with the cone angle, while the orthogonal to the plane component behaves as the second Legendre polynomial, possesses a zero at $\cos\theta_c = 1/\sqrt{3}$, and changes the orientation for the wider cone angle.

For the linearly polarized twisted radiation the results are even more intriguing: similar to plane-wave radiation, the spin is orthogonal to the electron emission direction, but a component oriented along the polarization vector, which does not exist in the conventional plane-wave case, appears.

As an illustrative example we consider photoionization of the $4p$ shell of atomic krypton in the dipole approximation within the jj-coupling scheme. It was found that even though the continuum is assumed to be smooth, some interesting spin polarization component patterns as a function of photoelectron polar emission angle θ_p and Bessel beam cone angle θ_c are observed. The more specific energy (spectroscopic) dependency is observed for the circularly polarized beam in the component oriented along the propagation direction. For the other component, energy dependency follows for the value of the dynamical parameters.

ACKNOWLEDGMENTS

The authors acknowledge A. Surzhykov for careful reading of the manuscript and useful suggestions. The work on the development of formalism for the photoelectron spin polarization in atomic ionization by twisted light and analysis in the case of the krypton atom was funded by the Russian Science Foundation (Project No. 23-62-10026 [77]). The calculations of the photoionization amplitudes were supported by the Ministry of Science and Higher Education of the Russian Federation (Project No. FEME-2024-0005) and Ministry of Science and Higher Education of the Russian Federation Grant No. 075-15-2021-1353.

[1] G. Molina-Terriza, J. P. Torres, and L. Torner, Twisted photons, Nat. Phys. **3**, 305 (2007).

[2] A. Bekshaev, K. Y. Bliokh, and M. Soskin, Internal flows and energy circulation in light beams, J. Opt. **13**, 053001 (2011).

[3] A. G. Peele, P. J. McMahon, D. Paterson, C. Q. Tran, A. P. Mancuso, K. A. Nugent, J. P. Hayes, E. Harvey, B. Lai, and I. McNulty, Observation of an x-ray vortex, Opt. Lett. **27**, 1752 (2002).

[4] S. Sasaki and I. McNulty, Proposal for generating brilliant x-ray beams carrying orbital angular momentum, Phys. Rev. Lett. **100**, 124801 (2008).

[5] E. Hemsing, A. Marinelli, and J. B. Rosenzweig, Generating optical orbital angular momentum in a high-gain free-electron laser at the first harmonic, Phys. Rev. Lett. **106**, 164803 (2011).

[6] U. D. Jentschura and V. G. Serbo, Compton upconversion of twisted photons: Backscattering of particles with non-planar wave functions, Eur. Phys. J. C **71**, 1571 (2011).

[7] U. D. Jentschura and V. G. Serbo, Generation of high-energy photons with large orbital angular momentum by Compton backscattering, Phys. Rev. Lett. **106**, 013001 (2011).

[8] J. He, X. Wang, D. Hu, J. Ye, S. Feng, Q. Kan, and Y. Zhang, Generation and evolution of the terahertz vortex beam, Opt. Express **21**, 20230 (2013).

[9] J. Bahrdt, K. Holldack, P. Kuske, R. Müller, M. Scheer, and P. Schmid, First observation of photons carrying orbital angular momentum in undulator radiation, Phys. Rev. Lett. **111**, 034801 (2013).

[10] Y. Shen, G. T. Campbell, B. Hage, H. Zou, B. C. Buchler, and P. K. Lam, Generation and interferometric analysis of high charge optical vortices, J. Opt. **15**, 044005 (2013).

[11] P. R. Ribič, D. Gauthier, and G. De Ninno, Generation of coherent extreme-ultraviolet radiation carrying orbital angular momentum, Phys. Rev. Lett. **112**, 203602 (2014).

[12] C. Hernández-García, L. Rego, J. San Román, A. Picón, and L. Plaja, Attosecond twisted beams from high-order harmonic generation driven by optical vortices, High Power Laser Sci. Eng. **5**, e3 (2017).

[13] K. Sueda, G. Miyaji, N. Miyanaga, and M. Nakatsuka, Laguerre-Gaussian beam generated with a multilevel spiral phase plate for high intensity laser pulses, Opt. Express **12**, 3548 (2004).

[14] M. Beijersbergen, R. Coerwinkel, M. Kristensen, and J. Woerdman, Helical-wavefront laser beams produced with a spiral phaseplate, Opt. Commun. **112**, 321 (1994).

[15] N. R. Heckenberg, R. McDuff, C. P. Smith, and A. G. White, Generation of optical phase singularities by computer-generated holograms, Opt. Lett. **17**, 221 (1992).

[16] E. Karimi, B. Piccirillo, E. Nagali, L. Marrucci, and E. Santamato, Efficient generation and sorting of orbital angular momentum eigenmodes of light by thermally tuned q-plates, Appl. Phys. Lett. **94**, 231124 (2009).

[17] J. Arlt and K. Dholakia, Generation of high-order Bessel beams by use of an axicon, Opt. Commun. **177**, 297 (2000).

[18] X. Cai, J. Wang, M. J. Strain, B. Johnson-Morris, J. Zhu, M. Sorel, J. L. O'Brien, M. G. Thompson, and S. Yu, Integrated compact optical vortex beam emitters, Science **338**, 363 (2012).

[19] H. Yang, Z. Xie, H. He, Q. Zhang, and X. Yuan, A perspective on twisted light from on-chip devices, APL Photonics **6**, 110901 (2021).

[20] R. M. Kerber, J. M. Fitzgerald, X. Xiao, S. S. Oh, S. A. Maier, V. Giannini, and D. E. Reiter, Interaction of an archimedean spiral structure with orbital angular momentum light, New J. Phys. **20**, 095005 (2018).

[21] E. I. Albar, F. P. Bonafé, V. P. Kosheleva, S. T. Ohlmann, H. Appel, and A. Rubio, Time-resolved plasmon-assisted generation of optical-vortex pulses, Sci. Rep. **13**, 14748 (2023).

[22] L. Allen, M. W. Beijersbergen, R. J. C. Spreeuw, and J. P. Woerdman, Orbital angular momentum of light and the transformation of Laguerre-Gaussian laser modes, Phys. Rev. A **45**, 8185 (1992).

[23] L. Allen, M. Padgett, and M. Babiker, *IV The Orbital Angular Momentum of Light* (Elsevier, New York, 1999), pp. 291–372.

[24] J. Durnin, Exact solutions for nondiffracting beams. I. The scalar theory, J. Opt. Soc. Am. A **4**, 651 (1987).

[25] J. Durnin, J. J. Miceli, and J. H. Eberly, Diffraction-free beams, Phys. Rev. Lett. **58**, 1499 (1987).

[26] M. Babiker, D. L. Andrews, and V. E. Lembessis, Atoms in complex twisted light, J. Opt. **21**, 013001 (2019).

[27] A. Surzhykov, D. Seipt, and S. Fritzsche, Probing the energy flow in Bessel light beams using atomic photoionization, Phys. Rev. A **94**, 033420 (2016).

[28] V. P. Kosheleva, V. A. Zaytsev, R. A. Müller, A. Surzhykov, and S. Fritzsche, Resonant two-photon ionization of atoms by twisted and plane-wave light, Phys. Rev. A **102**, 063115 (2020).

[29] S. Ramakrishna, J. Hofbrucker, and S. Fritzsche, Photoexcitation of atoms by cylindrically polarized Laguerre-Gaussian beams, Phys. Rev. A **105**, 033103 (2022).

[30] F. Araoka, T. Verbiest, K. Clays, and A. Persoons, Interactions of twisted light with chiral molecules: An experimental investigation, Phys. Rev. A **71**, 055401 (2005).

[31] A. A. Peshkov, S. Fritzsche, and A. Surzhykov, Ionization of H_2^+ molecular ions by twisted Bessel light, Phys. Rev. A **92**, 043415 (2015).

[32] O. Matula, A. G. Hayrapetyan, V. G. Serbo, A. Surzhykov, and S. Fritzsche, Atomic ionization of hydrogen-like ions by twisted photons: Angular distribution of emitted electrons, J. Phys. B: At., Mol. Opt. Phys. **46**, 205002 (2013).

[33] D. Seipt, R. A. Müller, A. Surzhykov, and S. Fritzsche, Two-color above-threshold ionization of atoms and ions in XUV Bessel beams and intense laser light, Phys. Rev. A **94**, 053420 (2016).

[34] A. Picón, J. Mompart, J. R. V. de Aldana, L. Plaja, G. F. Calvo, and L. Roso, Photoionization with orbital angular momentum beams, Opt. Express **18**, 3660 (2010).

[35] S. A.-L. Schulz, S. Fritzsche, R. A. Müller, and A. Surzhykov, Modification of multipole transitions by twisted light, Phys. Rev. A **100**, 043416 (2019).

[36] M. D. Kiselev, E. V. Gryzlova, and A. N. Grum-Grzhimailo, Angular distribution of photoelectrons generated in atomic ionization by twisted radiation, Phys. Rev. A **108**, 023117 (2023).

[37] J. W. Cooper, Multipole corrections to the angular distribution of photoelectrons at low energies, Phys. Rev. A **42**, 6942 (1990).

[38] S. A. Wolf, D. D. Awschalom, R. A. Buhrman, J. Daughton, S. von Molnar, M. L. Roukes, A. Chtchelkanova, and D. Treger, Spintronics: A spin-based electronics vision for the future, Science **294**, 1488 (2001).

[39] N. Rougemaille and A. Schmid, Magnetic imaging with spin-polarized low-energy electron microscopy, Eur. Phys. J. Appl. Phys. **50**, 20101 (2010).

[40] P. D. Johnson, Spin-polarized photoemission, Rep. Prog. Phys. **60**, 1217 (1997).

[41] U. Heinzmann and J. H. Dil, Spin-orbit-induced photoelectron spin polarization in angle-resolved photoemission from both atomic and condensed matter targets, J. Phys.: Condens. Matter **24**, 173001 (2012).

[42] B. Lv, T. Qian, and H. Ding, Angle-resolved photoemission spectroscopy and its application to topological materials, Nat. Rev. Phys. **1**, 609 (2019).

[43] K. Meng, L. Guo, and X. Sun, Strategies and applications of generating spin polarization in organic semiconductors, Nanoscale Horiz. **8**, 1132 (2023).

[44] U. Fano, Spin orientation of photoelectrons ejected by circularly polarized light, Phys. Rev. **178**, 131 (1969); Spin orientation of photoelectrons: Erratum and addendum, **184**, 250 (1969).

[45] M. S. Lubell and W. Raith, Polarization effect in photoionization of cesium, Phys. Rev. Lett. **23**, 211 (1969).

[46] J. Kessler and J. Lorenz, Experimental verification of the Fano effect, Phys. Rev. Lett. **24**, 87 (1970).

[47] N. Cherepkov, Spin polarization of atomic and molecular photoelectrons, in *Advances in Atomic and Molecular Physics*, Advances in Atomic and Molecular Physics, edited by D. Bates and B. Bederson (Academic Press, New York, 1983), Vol. 19, pp. 395–447.

[48] N. Cherepkov, Spin polarisation of photoelectrons ejected from unpolarised atoms, J. Phys. B: At. Mol. Phys. **12**, 1279 (1979).

[49] N. Cherepkov, Spin polarisation of electrons ejected from unpolarised atoms by unpolarised and linearly polarised light, J. Phys. B: At. Mol. Phys. **11**, L435 (1978).

[50] I. Barth and O. Smirnova, Spin-polarized electrons produced by strong-field ionization, Phys. Rev. A **88**, 013401 (2013).

[51] D. B. Milošević, Possibility of introducing spin into attoscience with spin-polarized electrons produced by a bichromatic circularly polarized laser field, Phys. Rev. A **93**, 051402(R) (2016).

[52] D. B. Milošević, Atomic and molecular processes in a strong bicircular laser field, Atoms **6**, 61 (2018).

[53] M.-M. Liu, Y. Shao, M. Han, P. Ge, Y. Deng, C. Wu, Q. Gong, and Y. Liu, Energy- and momentum-resolved photoelectron spin polarization in multiphoton ionization of Xe by circularly polarized fields, Phys. Rev. Lett. **120**, 043201 (2018).

[54] N. M. Kabachnik and I. P. Sazhina, Spin polarization of electrons in two-color XUV + optical photoionization of atoms, Atoms **10**, 66 (2022).

[55] E. V. Gryzlova, M. M. Popova, and A. N. Grum-Grzhimailo, Spin polarization of photoelectrons in bichromatic extreme-ultraviolet atomic ionization, Phys. Rev. A **102**, 053116 (2020).

[56] M. M. Popova, E. V. Gryzlova, M. D. Kiselev, and A. N. Grum-Grzhimailo, Symmetry violation in bichromatic ionization by a free-electron laser: Photoelectron angular distribution and spin polarization, Symmetry **13**, 1015 (2021).

[57] M. M. Popova, E. V. Gryzlova, M. D. Kiselev, and A. N. Grum-Grzhimailo, Ionization of atoms by a bichromatic fields

of $\omega+\ 2\omega$ multiple frequencies with arbitrary polarization, J. Exp. Theor. Phys. **135**, 58 (2022).

[58] S. Svensson, B. Eriksson, N. Mårtensson, G. Wendin, and U. Gelius, Electron shake-up and correlation satellites and continuum shake-off distributions in x-ray photoelectron spectra of the rare gas atoms, J. Electron Spectrosc. Relat. Phenom. **47**, 327 (1988).

[59] S. A.-L. Schulz, A. A. Peshkov, R. A. Müller, R. Lange, N. Huntemann, C. Tamm, E. Peik, and A. Surzhykov, Generalized excitation of atomic multipole transitions by twisted light modes, Phys. Rev. A **102**, 012812 (2020).

[60] G. F. Quinteiro, D. E. Reiter, and T. Kuhn, Formulation of the twisted-light–matter interaction at the phase singularity: The twisted-light gauge, Phys. Rev. A **91**, 033808 (2015).

[61] G. F. Quinteiro, C. T. Schmiegelow, D. E. Reiter, and T. Kuhn, Reexamination of Bessel beams: A generalized scheme to derive optical vortices, Phys. Rev. A **99**, 023845 (2019).

[62] V. V. Balashov, A. N. Grum-Grzhimailo, and N. M. Kabachnik, *Polarization and Correlation Phenomena in Atomic Collisions* (Springer US, Boston, 2000).

[63] H. M. Scholz-Marggraf, S. Fritzsche, V. G. Serbo, A. Afanasev, and A. Surzhykov, Absorption of twisted light by hydrogenlike atoms, Phys. Rev. A **90**, 013425 (2014).

[64] N. M. Kabachnik, Modern studies of anisotropy and polarization in auger-electron emission, in *Electron and Photon Impact Ionization and Related Topics 2004*: *Proceedings of the International Conference Louvain-la-Neuve, 1-3 July 2004*, 1st ed., edited by B. Piraux (Institute of Physics Publishing, Bristol and Philadelphia, 2005), pp. 33–44.

[65] C. F. Fischer, T. Brage, and P. Johnsson, *Computational Atomic Structure: An MCHF Approach* (IOP Publishing, Bristol, 1997).

[66] O. Zatsarinny and K. Bartschat, The *B*-spline *R*-matrix method for atomic processes: Application to atomic structure, electron collisions and photoionization, J. Phys. B: At. Mol. Opt. Phys. **46**, 112001 (2013).

[67] O. Zatsarinny, BSR: *B*-spline atomic *R*-matrix codes, Comput. Phys. Commun. **174**, 273 (2006).

[68] S. Fritzsche, A. N. Grum-Grzhimailo, E. V. Gryzlova, and N. M. Kabachnik, Sequential two-photon double ionization of Kr atoms, J. Phys. B: At., Mol. Opt. Phys. **42**, 145602 (2009).

[69] D. L. Miller, J. D. Dow, R. G. Houlgate, G. V. Marr, and J. B. West, The photoionisation of krypton atoms: A comparison of pseudopotential calculations with experimental data for the 4p asymmetry parameter and cross section as a function of the energy of the ejected photoelectrons, J. Phys. B **10**, 3205 (1977).

[70] U. Fano and J. W. Cooper, Line profiles in the far-uv absorption spectra of the rare gases Phys. Rev. **137**, A1364 (1965).

[71] U. Hahn, J. Semke, H. Merz, and J. Kessler, Spin polarisation and angular distribution measurement of MNN Auger electrons from krypton and xenon, J. Phys. B **18**, L417 (1985).

[72] K. Blum, B. Lohmann, and E. Taute, Angular distribution and polarisation of Auger electrons, J. Phys. B **19**, 3815 (1986).

[73] B. Lohmann, Analyses and model calculations on the angular distribution and spin polarization of Auger electrons, J. Phys. B: At., Mol. Opt. Phys. **23**, 3147 (1990).

[74] N. M. Kabachnik and I. P. Sazhina, Angular distribution and spin polarisation of Auger electrons, J. Phys. B **17**, 1335 (1984).

[75] N. M. Kabachnik and I. P. Sazhina, Model calculation of Auger-electron spin polarization, Optics and Spectroscopy (English translation of Optika i Spektroskopiya) **60**, 1106 (1986).

[76] N. M. Kabachnik and I. P. Sazhina, Spin-polarized Auger-electron spectroscopy of the d atomic shell. Model calculation for noble-gas atoms, J. Phys. B: At., Mol. Opt. Phys. **21**, 267 (1988).

[77] https://rscf.ru/en/project/23-62-10026/.